Corrosion Inhibition Performance of *Brachystegia eurycoma* Leaf Extract on Mild Steel in Acid Media

L. N. Emembolu [a], F. U. Iwuchukwu [a], C. C. Ejiofor [a*], J. J. Ajali [a] and C. E. Chinyelu [a]

[a] Department of Chemical Engineering, Nnamdi Azikiwe University Awka, Anambra state, Nigeria.

Authors' contributions

This work was carried out in collaboration among all authors. All authors read and approved the final manuscript.

Original Research Article

ABSTRACT

The aim of this work is to investigate the corrosion inhibition of *B. eurycoma* leaves extract as a natural inhibitor for mild steel corrosion in 3 M H_2SO_4 solution. The corrosion inhibitory activity was analyzed by electrochemical impedance spectroscopy (EIS) and potentiodynamic polarization. The surface roughness and its properties through scanning electron microscopy (SEM). The obtained result from EIS divulges that the gradual increase in inhibitor concentration and time of immersion leads to progressive increase in inhibition efficiency. At the end of 8 hours immersion time and inhibitor concentration of 1000 mg/l the highest inhibition efficiency of (88%) was obtained. The potentiodynamic polarization results indicated that addition of *B. eurycoma* leaves extracts hindered the reaction rates of anodic and cathodic reactions thereby performing as mixed- type inhibitor. The corrosion current density also revealed that in the presence of *B. eurycoma* leaves extracts the value of corrosion density reduced considerably from 265.2μA/cm^2 for sample without inhibitor to 67.8μA/cm^2 for sample with inhibitor. Again, it was observed that in the presence *B. eurycoma* leaves extracts the mechanism of hydrogen (effervescence) evolution was unique whereas the

_____

Corresponding author: Email: cc.ejiofor@unizik.edu.ng;

anodic dissolution of iron mechanism experienced the impact of the inhibitor. SEM inspection revealed that the mild steel surface showed smoother and lower damage in the presence of inhibitor. Obvious correlations were found between corrosion inhibition efficiency and some quantum chemical parameters such as energy of highest occupied molecular orbital (E_{HOMO}), energy of lowest unoccupied molecular orbital (E_{LUMO}), energy gap (E_{L-H}) and electronic density etc. The obtained results were further elucidated with frontier molecular orbital theory.

ABBREVIATIONS

MS   : Mild Steel
EIS   : Electrochemical Impedance Spectroscopy
PDP   : Potential Dynamic Polarization
SEM   : Scanning Electron Microscopy
FT-IR   : Fourier Transform Infrared
DFT   : Density Functional Theory
MD   : Molecular Dynamics
OCP   : Open Circuit Potential
EHOMO   : Energy of Highest Occupied Molecular Orbital
ELUMO   : Energy of the Lowest Unoccupied Molecular Orbital
HOMO   : Highest Occupied Molecular Orbital
LUMO   : Lowest Unoccupied Molecular Orbital
COMPASS   : Condensed Phase Optimized Molecular Potentials for Atomistic Simulation Studies
CPEt   : Constant Phase Element
Rct   : Charge Transfer Resistance
Ct   : Double Layer Capacitance
Kads   : Equilibrium Constant
⊿Goads   : Standard Energy Free of Adsorption
Ea   : Apparent Activation Energy
Eads   : Adsorption Energy
EL-H   : Reduced Energy Gap

1. INTRODUCTION

Mild steel is useful in engineering constructions and in chemical industries due to its mechanical characterization and wide range of applications like structural materials for pipelines, vessels and industrial tools that easily corrode when in contact with solvents [1, 2]. Most acid solutions used for cleaning, acid descaling metal etching and other acidic operations have potentials of causing damage to the metal surface, and the use of organic originated inhibitors has been reported as one of the greatest options amongst others for prevention of corrosion in metals [1, 3, 4]. Hydrochloric acid, sulfuric acid and nitric acid are the most frequently used acids. The alloys of iron and iron are reactive materials with high potency of corroding in acidic solutions and inhibitor addition protects them from acid damages [5]. Generally, interactions between metals and the acidic medium used expose industrial facilities and equipment to corrosion

thereby causing unfavorable economic implications [3]. The important characteristics of materials and structures like appearance, gas and liquid permeability & strength is downgraded by corrosion and hence reduces the material's utility efficiency [6]. As regards the current economy of the nation and financial burden caused by corrosion damages, several researchers [6-8] has explored possible methods of improving metal resistance.

Corrosion inhibitors are chemical compounds that decreases the rate of corrosion in a material when added to either liquids or gases [3, 6]. The efficiency of a corrosion inhibitor is dependent on factors like quantity of water, flow regime and the fluid composition. They could also be used as additives to fluids surrounding the metals [1, 6]. Inhibitors improves performance of materials and age of the equipment without altering the process technology [7]. Previous works done by researchers [8-11] on increasing the efficiency of

organic compounds with hetero-atoms traces as corrosion inhibitors for mild steel in acidic medium was reported by Olofinjana et al [6]. In processes for corrosion prevention caused by free electron pairs, the contact between hetero-atoms like oxygen, nitrogen, phosphorus, Sulphur and double/triple bond in the form of a wall and mild steel plays an important part. More so, as a result of the environmental damages caused by synthetic induced corrosion inhibitors, investigation of natural products from plant origin as corrosion inhibitors has greatly increased due to their ecofriendly and cost-effective characteristics. The plant originated products are also biodegradable, nontoxic and renewable materials [8]. Ozoemena, Akpan [6] recorded several plant extracts like Gliricidia sepium, Azadirachta indica, Pterocarpus soyauxii Taul, Momordica charantia and Boscia senegalensis that has been initially explored as corrosion inhibitors. Recently, the effect of kalmegh leaf extract on the corrosion behavior of aluminum alloy in 1M NaOH solution was investigated using, potentiodynamic polarization, and electrochemical impedance spectroscopy (EIS) techniques. The results obtained showed that the inhibitor acts as a mixed type, controlling both the anodic and the cathodic reactions. Also, the maximum inhibition efficiency of 82.24 and 82.45% from EIS and PDP studies, respectively, were achieved at higher concentration by Namrata, et al, [12]. Equally, Onyenanu et al, [13] worked on *A. mossambicensis* and *E. sonchifolia* Leaves' Extracts on Aluminum in Alkaline Media using Gravimetric and Electrochemical measurements obtained maximum inhibition efficiency of 79.04 and 77.00% each in KOH and NaOH respectively. In the last decades or more, plant extracts have been widely acknowledged as Corrosion inhibitors [11-12] due to easy and low-cost extraction, efficacy, availability and ecofriendly. Though, it is equally important to investigate the effectiveness of the plant extract to be used as corrosion inhibitors in terms of its adsorption mechanisms. Again, due to abundance of Phyto molecules like flavonoids, terpenoids, amino acids, phenolic compounds and alkaloids etc., in the ethanolic extracts of *Brachystegia eurycoma* extract. As a result, this work was embarked upon to explore the potentials of B. eurycoma leaves extracts as a green corrosion inhibitor in acid solution.

Brachystegia eurycoma (widely identified as Achi in the eastern part of Nigeria) widely grown in the tropical rain forest of West Africa. In Eastern part of Nigeria, the edible seed serves as a thickener in one of their famous local soups, functional agents in formulation of meats and in bakery products. Furthermore, the seed also possesses antimalarial, anti-inflammatory, anti-corrosion and anti-diabetics features. Computational methods have been used extensively in several fields using software development approach and visible in the use of quantum chemical calculations for corrosion studies [14-18]. B. eurycoma leaves extract were used here as viable corrosion inhibitors, and the inhibition performance were evaluated. As a result of its outstanding features like high solubility, good adsorption capability, robust affinity etc., the produced extracts were regarded as eco-friendly corrosion inhibitors which influences the chemical and physical procedures of electrochemical corrosion behaviors through stimulating the formation of a protective layer on the metal surface. Furthermore, B. eurycoma leaves extract can be seen as a group of heterocyclic compounds comprising of one or more heteroatoms, aromatic rings and polar functional groups. Also, the capability as H-bond acceptors and donors, and the π-conjugated molecular structure of the extracted inhibitors adds to the strength of organic layers development during adsorption on the mild steel (MS) surfaces [19-22]. The behavioral performance of *B. eurycoma* leaves extract was evaluated in this current work using electrochemical impedance spectroscopy (EIS), potentiodynamic polarization (PDP) studies. Equally, the morphologies of the surfaces were evaluated using scanning electron microscopy (SEM) and Fourier-transform infrared (FT-IR) analysis. Interactions with the steel surface and the adsorption configuration of the inhibitor molecules was also clarified. Verification of the reactivity of the inhibitor molecules in terms of the charge-transfer ability, adsorption energy of the selected constituents and confirmation of the experimental results were carried out by density functional theory (DFT) and molecular dynamics (MD) simulations

2. MATERIALS AND METHODS

2.1 Materials Collections and Preparations

2.1.1 Metal Preparation

The mild steel sheet was mechanically cut into coupons with dimensions 3cm x 8cm x 0.2cm. The coupons were polished with sand papers of

different grades of coarseness from 200-1000, cleaned with distilled water and ethanol, and then dried with dryer.

2.1.2 Collection and preparation of *B. eurycoma* leaves

B. eurycoma leaves used in this work was collected from a village called Ngene-Ugbo in Enugu State and identified in the Department of Botany, Nnamdi Azikiwe University Awka. The leaves were rinsed in distilled water thrice, sun dried for 48 hours and ground into powder. The *B. eurycoma* leaves extract was prepared by concentrating in a rotary evaporator after obtaining the extract from Soxhlet extraction with 99% C_2H_5OH at 75 °C. The *B. eurycoma* leaves extract was stowed in 5°C refrigerator and used as a corrosion inhibitor for mild steel in H_2SO_4 solutions. The functional groups of the *B. eurycoma* leaves extracts was identified by FTIR analyzer.

2.1.3 Test solutions

Reagents used in the current work were obtained from Top Divine Scientific Ltd, Head Bridge Onitsha market without further treatment. The corrosion experiments were done in 3 M H_2SO_4 solution in the absence and presence of various *B. eurycoma* concentrations. The 3 M H_2SO_4 solutions were prepared with 98% purity H_2SO_4 solution and distilled water. Analytical-grade chemical reagents and distilled water were used in preparing all the test solutions. Freshly prepared solution was used for each experiment. The pressure and temperature of the experiments were controlled by opening the test solutions to the atmosphere and maintaining the temperature at 298 K thermostatically.

2.2 Methods

2.2.1 Instrumental analysis

2.2.1.1 Fourier Transform Infrared Spectroscopy (FTIR) study

The functional groups in major components of *B. eurycoma* leaves extract were examined using FTIR analyzer. Identification of the functional groups in the organic components was done by Thermo Fisher Nico-let iS10 instrument within the range of 600 – 4567 cm^{-1} wave number and were shielded by *B. eurycoma* leaves extracts respectively.

2.2.1.2 Surface morphology examination

The inspection of surface morphology on the inhibited and uninhibited species were done using SEM. Surface analysis was conducted by SEM model Philips XL30 microscope. Analysis of contact angle were carried out by utilizing OCA 15 plus type system.

2.2.2 Electrochemical measurements

Electrochemical impedance spectroscopy (EIS) and Potentiodynamic polarization (PDP) measurements were done by employing GILL AC attached to a software known as "gill". The fitting and associated parameters were obtained through Z-view software package. All experiments were done in a cell with three electrode configuration: The mild steel (MS) specimen was the working electrode, with the saturated calomel electrode being the reference electrode and platinum sheet with 2 cm^2 surface area as the electrode. The samples were immersed in 3 M H_2SO_4 solution for 30 mins at room temperature to establish the steady state open circuit potential (OCP) Fig 1. After measuring the OCP the electrochemical measurements were performed. The polarization measurements were done by scanning the potential in the range of –250 to +250mV at $1mVs^{-1}$. The EIS results were obtained over a frequency range of 0.01Hz to 10 kHz with 10mV amplitude. The equations (1) and (2) were used in the calculating the corrosion inhibition efficiency based on polarization ($\eta_{polarization}$) and EIS (η_{EIS}) results [19]:

$$\eta_{polarization} = \left(1 - \frac{i_{corr}}{i_{corr}^\circ}\right) \times 100 \qquad (1)$$

$$\eta_{EIS} = \left(1 - \frac{R_{ct}^\circ}{R_{ct}}\right) \times 100 \qquad (2)$$

Where the i°_{corr} and i_{corr} is the corrosion current densities of the samples subjected to the H_2SO_4 solution and the electrolyte protected by *B. eurycoma* leaves extracts, respectively. Similarly, the parameters of R°_{ct} and R_{ct} is the resistance related to charge transfer without and with *B. eurycoma* leaves extract. The electrochemical measurements were conducted within the concentration range of 0, 200 and 1000mg/L respectively, basically to determine the effect of *B. eurycoma* leaves extracts at elevated concentrations at room temperature.

2.2.3 Quantum studies

Theoretical calculations were performed with Gaussian 03, E.01, and software. The electrons/atoms calculations of the inhibitor molecules were conducted by the density functional theory (DFT)/B3LYP method [20]. Analysis of information about molecular geometric and electron distributions as well as inhibitor efficiencies and inhibitor/surface interactions due to its accuracy and less time requirement from the computational point of view was validated with DFT [20-21]. All the geometric variables without any symmetry constraints for the geometries of all studied inhibitors were optimized. On the other hand, no imaginary frequency was recorded after Frequency calculation indicating the existence of minimum-energy structures. Hence, the application of Koopman's theorem (1, 3) was useful in evaluating the electronic properties such as electron affinity (A) and ionization potential (I) because it provides relationship between the electron affinity, the ionization potential and the energies (i.e. the energy of highest occupied molecular orbital E_{HOMO}, energy of the lowest unoccupied molecular orbital E_{LUMO}), highest occupied molecular orbital HOMO, and the lowest unoccupied molecular orbital LUMO and ($\Delta E_{L-H} = E_{LUMO} - E_{HOMO}$) correspondingly. Furthermore, A and I are related to E_{HOMO} and the E_{LUMO} as shown in the Eqs. (3) and (4) below; [20, 22 -24] [9].

$$I = -E_{HOMO} \tag{3}$$

$$A = -E_{LUMO} \tag{4}$$

The absolute hardness, η, and absolute electronegativity, χ, of the inhibitor molecule were calculated as;

$$\chi = \frac{I+A}{2} = -\frac{E_{HOMO}+E_{LUMO}}{2} \tag{5}$$

$$\eta = \frac{I-A}{2} = \frac{E_{LUMO}-E_{HOMO}}{2} = \frac{1}{2}\Delta E_{L-H} \tag{6}$$

The global softness, σ, can also be defined as follows:

$$\sigma = \frac{1}{\eta} \tag{7}$$

$$N = \frac{-\chi_{inhibitor}}{2\eta_{inhibitor}} \tag{8}$$

The fraction of electrons transferred from the inhibitor molecule to the metallic atom (ΔN) was calculated according to Pearson from the obtained values of χ and η. For the calculation the following formula was used:

$$\Delta N = \frac{\phi-\chi_{inhibitor}}{2\eta_{inhibitor}} = \frac{\chi_{Fe}-\chi_{inhibitor}}{2(\eta_{Fe}+\eta_{inhibitor})} \tag{9}$$

Using a theoretical value in Eq. (11) the work function of iron (ϕ) was substituted with its electronegativity $\chi_{Fe} = 7eV$ and a global hardness of $\eta_{Fe} = zero$, by assuming that for a metallic bulk I = A, because they are softer than the neutral metallic atoms [9][25]. Additionally, DFT code

2.2.4 Molecular simulations

Molecular dynamic (MD) simulation as an efficient and reliable technique was utilized in this work to elucidate the experimental findings, and throw more light on the existence of thermonuclear adsorption of the *B. eurycoma* leaves extract (components) on the metal substrate.

Forcite molecular dynamics was employed to calculate different energy of adsorption configurations of molecule on Fe surface. The Fe surface was cleaved along the (110) plane because it has a density packed surface and the most stabilization is carried out at this position. Calculations were carried out in a 12 x 10 super cell using the COMPASS (Condensed phase optimized molecular potentials for atomistic simulation studies) force field and the smart algorithm with NVT canonical ensemble, a time step of 1fs, and simulation time 5000 ps is in line with [26-27]. The interactions and binding energies of the *B. eurycoma* leaves inhibitor with the Fe (110) surface in the simulation system, were assessed using the following Eq. [24]:

$$E_{interaction} = E_{total} - \left(E_{surface + solution} + E_{inhibitor}\right) \tag{10}$$

$$E_{binding} = -E_{interaction} \tag{11}$$

where $E_{surface + solution}$ is assigned to the total energy of Fe (1 1 0) surface and solution without the inhibitors; $E_{inhibitor}$ indicate the total energy of inhibitors and E_{total} represents the total energy of the whole system.

3. RESULTS AND DISCUSSION

3.1 Electrochemical Measurements

3.1.1 Electrochemical Impendence Spectroscopy (EIS)

The special effects of *B. eurycoma* leaves extract concentration on inhibition of mild steel was investigated by electrochemical impedance spectroscopy and potential dynamic polarization methods. The impedance measurements between Mild Steel-H_2SO_4 acid interface in the absence and presence of optimal concentration of *B. eurycoma* leaves extract was determined by OCP. The Open circuit potential (OCP), as a function of time for Mild steel in 3 M H_2SO_4 in containing different concentrations of *B. eurycoma* leaves extract were presented in Fig. 1. It can be seen clearly from Fig.1 that increase in the concentrations of *B. eurycoma* leaves extract and immersion time caused gradual shift of OCP to more negative values. It is equally observable that the highest negative OCP values occurred in MS coupons immersed in 3 M H_2SO_4 containing 200 mg/L of *B. eurycoma* leaves extract. The obtained results can be attributed to the adsorption of inhibitors molecules on the MS surface which resulted in shift of OCP to more negative values.

Also, Modeling of the impedance plots and extraction of electrochemical parameters was done with one-time constant electrical equivalent circuit (R(R/Q)) shown in Fig. 2. The model consists of R_t, R_s and CPE_t as solution resistance. Therefore, total resistance, (R_t = charge transfer resistance (Rct) + inhibitor film resistance (R_f)) and constant phase element Y_0, (CPE_t) respectively. The charge transfer resistance (Rct) is in parallel with CPE while both are in series with solution resistance. The goodness of fit of the equivalent circuit for the EIS measurements onto the inhibited metal surfaces was performed with the help of Chi square. Hence, the accuracy of the equivalent circuit used was evaluated based on Chi square (χ^2) values obtained as in Table 1. The inhibition was obtained from Eq. (2). Therefore, the Double layer capacitance (C_t) data was evaluated using Eq. (12); [16, 28-32].

$$C_t = \frac{(R_p \times Y_0)^{\frac{1}{n}}}{R_p} \qquad (12)$$

Where Y_0 is the Proportionality constant, R_t is the Polarization resistance, τ is the phase angle of CPE. "n" is fractional exponent for solid electrodes/solution interfaces and its value is $-1 \leq n \leq 1$ [28].
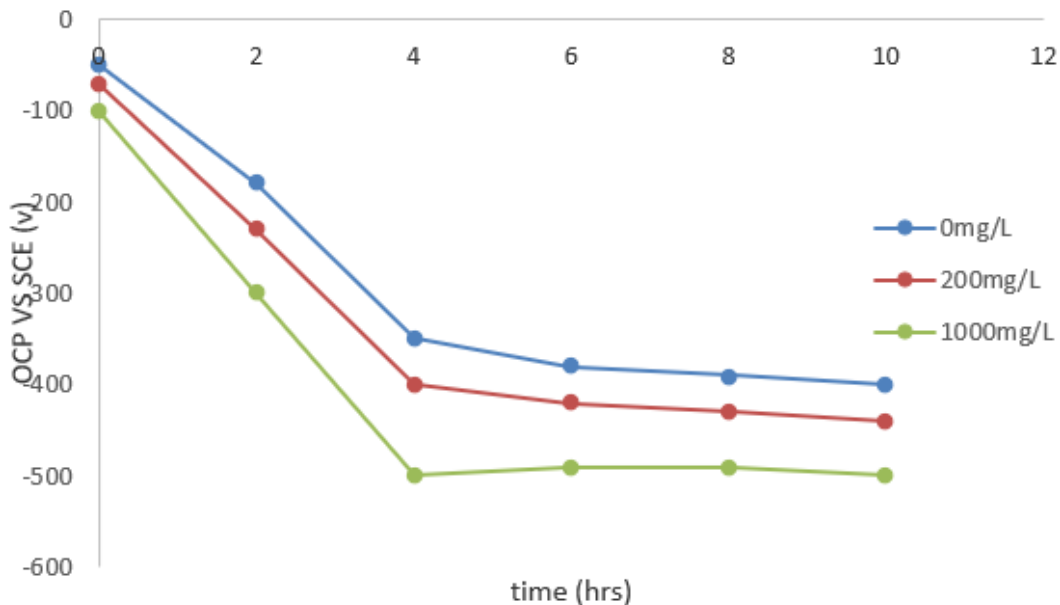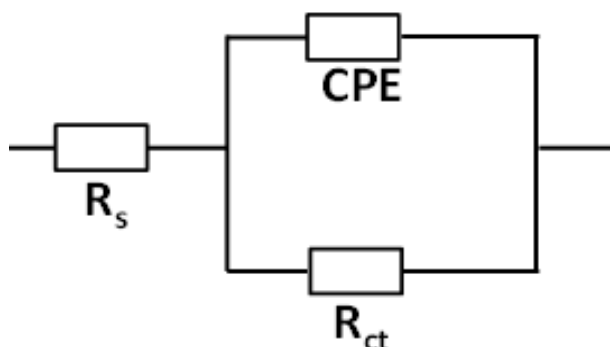

Fig. 1. OCP as a function of time for MS coupons in H_2SO_4 with and without different concentrations of *B. eurycoma* leaves extract

Fig. 2. Equivalent circuit model for mild steel with the accompanying experimental fit

The diagrams in Fig. 3 (a-c) demonstrated that the behavior of the of blank solution remained constant during and after 8 hours immersion time implying that there is only one time constant in all the plots which can be as a result of charge transfer resistance controlling the corrosion reaction. Also, the shape of the semicircular graph called Nyquist plot remained unaffected after progressive increasing the concentration of *B. eurycoma* leaves extract to 1 M H_2SO_4. This inference can be attributed to the corrosion mechanism been adamant regardless of the absence or presence of *B. eurycoma* leaves extracts. Again, the diameter of Nyquist plots increases by increasing both the inhibitors concentration and the immersion time which can be attributed to the existence of adsorbed organic compounds from *B. eurycoma* leaves extract on mild steel surface thereby consolidating the formation of the inhibitive film. Table 1 shows that increase in the concentrations of *B. eurycoma* leaves extract increases the value of R_t. Also, increase in immersion time leads to increase in low frequency impendence ($|Z|_{10\ mHz}$) and R_t values in the presence of different concentrations of *B. eurycoma* leaves extract. Similarly, the maximum high frequency angle($\theta_{10\ kHz}$), ($|Z|_{10\ mHz}$) and R_t were achieved in the presence of 1000 mg/L *B. eurycoma* leaves extract indicating the high

surface coverage of adsorbed inhibitor molecules. Inferences from Table 1 indicates gradual increase in "n" which resulted from increase in the concentrations of *B. eurycoma* leaves extract and immersion time. This can be as a result of decline in the surface roughness and inhomogeneity caused by adsorption of inhibitor molecules [33-35]. Table 1 points out that increase in phase angle resulted from increase in the inhibitor concentration and this is as a result of reduction in surface irregularities due to adsorption of organic molecules *B. eurycoma* leaves extract on the Mild steel [36-37].

Here, it is noteworthy that the gradual increase in the inhibitor concentration and immersion time resulted in the substantial decrease of double layer capacitance which leads to increase in the protective film thickness and causing a decrease in the dielectric constant. Fig. 3(b) shows Bode plots have a solitary peak indicating that electrochemical impedance measurements is appropriate for one time constant equivalent model. Furthermore, Fig. 3(c), presents a substantial increase in phase angle value compared to the blank solution which is attributable to capacitive response of adsorption of the inhibitor molecules on the metal surface.

Table 1. Impedance parameters obtained from mild steel corrosion in 3 M H_2SO_4 with and without different concentrations of *B. eurycoma* leaves extracts

System	Immersion Time (hr.)	R_t (Ωcm^2)	$Y_{0,t}$ ($\mu s^n \Omega^{-1} cm^{-2}$)	n_t	C_t ($\mu F cm^{-2}$)	τ (ms)	Log$|Z|$ (Ωcm^2)	Phase angle (°)	η_{EIS} (%)	χ^2
Blank	2	133	177	0.88	67.3	8.3	2.4	1.4	-	0.000078
200mg/L B	6	346	52.8	0.89	33	12	2.5	14.2	84	0.00045
1000mg/LB	8	1263	34.1	0.90	20.2	16	2.9	25.3	85	0.00056

It is equally observable from Table 1, that increase in the inhibitors concentration and immersion time causes a substantial decrease in the values of double layer capacitance implying that the reduction in dielectric constant is due to the replacement of water molecules with the inhibitor molecules. [38-40].

3.1.2 Potentiodynamic Polarization (PDP)

The potentiodynamic polarization studies was done to determining the consequences of *B. eurycoma* leaves extract on the cathodic hydrogen ion reduction reaction and anodic dissolution of mild steel in H_2SO_4 solution. Fig 4. Shows the PDP curves of MS in 1 M H_2SO_4 with and without the *B. eurycoma* leaves extracts and discloses that the addition of the *B. eurycoma* leaves extracts influences the cathodic hydrogen evolution processes and the anodic metallic dissolution. It is important to note that, the existence of the *B. eurycoma* leaves extracts moved both the cathodic and anodic polarization curves to lower current densities, that is, towards lower rates of MS corrosion. The outcome of the above result is more prominent by increasing *B. eurycoma* leaves extracts concentration. Hence, the electrochemical potentio-kinetic parameters of MS corrosion were determined using the Tafel extrapolation method, see Table 2. The electrochemical parameters comprise of the corrosion current density (i_{corr}), corrosion potential (E_{corr}) for samples in the absence and presence of inhibitors at different concentrations, slopes of the anodic and cathodic branches (βa and βc), and inhibition efficiency (η%). Therefore, η% was calculated using Eq. (1). Thus, increased η% resulted from reduction in current density (i_{corr}) caused by increasing the concentration of inhibitors see Table 2. Again, it is observable from Table 2, that the values of E_{corr} in the presence of the *B. eurycoma* leaves extracts were significantly decreased to more negative values when compared with the values obtained in the absence of inhibitors. This suggests that the inhibition for anodic reaction, that is, iron dissolution is more resilient than the cathodic reaction, that is, evolution of hydrogen. This can be attributed to formation a protective film which causes a considerable decrease in the volume of corrosive ingredients from adhering on the substrate that is, metal. Furthermore, in the presence of the inhibitors the MS surface experienced greater corrosion resistance than in the absence of the inhibitors. However, an inhibitor can be either anodic or cathodic, if the value of E_{corr} is higher than -85mV per SCE in

comparison with corrosion potential of uninhibited solution, while on the other hand, an inhibitor can be mixed-type, if the value of E_{corr} is lower than -85mV per SCE [53-54]. In this work, the shift is less than -85mV per SCE suggesting that the studied inhibitor is mixed-type inhibitor. The mixed-type nature of *B. eurycoma* leaves extracts was further affirmed by slight alterations in βa and βc values dues to increase in inhibitor concentration indicating that the *B. eurycoma* leaves extracts worked through a mixed adsorption mechanism. Besides all these, the inhibitor simply works by shielding or blocking the energetic spots on the metal surface [14, 37- 40]. It is noteworthy that the authors did not consider concentrations within range of 400-800ppm because the most literatures contain enough information within the listed range and can be seen from our previous work with different inhibitors [37]. However, at elevated concentrations for instance, 1000g/L the reaction mechanism was not affected as previously as discussed [41-42].

3.2 Adsorption Isotherm Considerations

It is widely accepted from literature, that the adsorption of inhibitor molecules on metal surface includes the removal of adsorbed water molecules via a displacement reaction. This occurs in such a way that as the adsorb ability and size of the inhibitor molecules increases as the solubility decreases. To further investigate the adsorption characteristics of *B. eurycoma* leaves extracts on the MS surface, the experimental results obtained from EIS and PDP measurements were fitted into Langmuir isotherm model Eq. (13), Fig. 5. Obviously, Fig 5 shows that Langmuir model is applicable to fit the data of the extract with high correlation coefficients ($R^2=1$) suggesting the ideal behavior of the adsorption process of the inhibitor unto the metal surface. Again, the values of the slopes Table 3 affirms that the inhibitor molecules were adsorbed on the MS surface in accordance with Langmuir adsorption model. The obtained K_{ads} values implied that *B. eurycoma* leaves extracts has high adsorption capability for the metal surface, that is, the better the K_{ads}, the tougher and more efficient the adsorbed layer on the steel surface and the greater the surface coverage [19]. The adsorption process of the *B. eurycoma* leaves extracts on the metal surface can be promising as disclosed by the negative values of ΔG_{ads} as well as its workability and spontaneous nature. The ΔG_{ads} values of - 25.16 and -21.42 $KJmol^{-1}$ implies that the adsorption

mechanism is physical and chemical adsorption (mixed adsorption) [54]. This observation is attributed to the fact that, negative values of ΔG_{ads} greater than 20 KJmol^{-1} is physical adsorption and less than 40 KJmol^{-1} is chemical adsorption, therefore, the ΔG_{ads} values of the studied inhibitor confirms the adsorption mechanism to be mainly physical adsorption.

$$\frac{C_{inh}}{\theta} = \frac{1}{K_{ads}} + C_{inh} \quad (13)$$

$$K_{ads} = \left(1/55.5\right) \times exp\left(-\Delta G_{ads}^{o}/RT\right) \quad (14)$$

Where, θ, is the degree of surface coverage on the metal surface, k_{ads}, is equilibrium constant, C, is inhibitor concentration, ΔG_{ads}^{o} is the standard energy free of adsorption and 55.5 is the molar water solution respectively.

3.3 Thermodynamic Study

Further insight on the adsorption process at the metal/ acid solution interface was through evaluation of the thermodynamic properties of the inhibitor. Hence, The Arrhenius and transition state equations were used to evaluate the temperature dependence [44]. The linearized form of Arrhenius and transition state equations were expressed in Eq. (14 and 15) respectively.

$$logK_{corr} = \frac{-E_a}{2.303RT} + logA \quad (15)$$

where E_a is the apparent activation energy, A is the pre-exponential factor, and R is the universal gas constant (8.314 J mol−1 K−1), T is absolute temperature and K_{corr} is corrosion rate. A plot of log K_{corr} against 1/T gives a straight line with A as the intercept and $\frac{E_a}{2.303RT}$ as slope in Fig. 6 from where the values of Ea were calculated. The obtained data in Table 4, reveals that the values of E_a decreased as the inhibitor concentration increases implying that the adsorption of the inhibitor on MS surface is by chemical adsorption [45]. The standard enthalpy $\Delta H^*$and the entropy of activation, ΔS^* were evaluated from Eq. (15) [47]
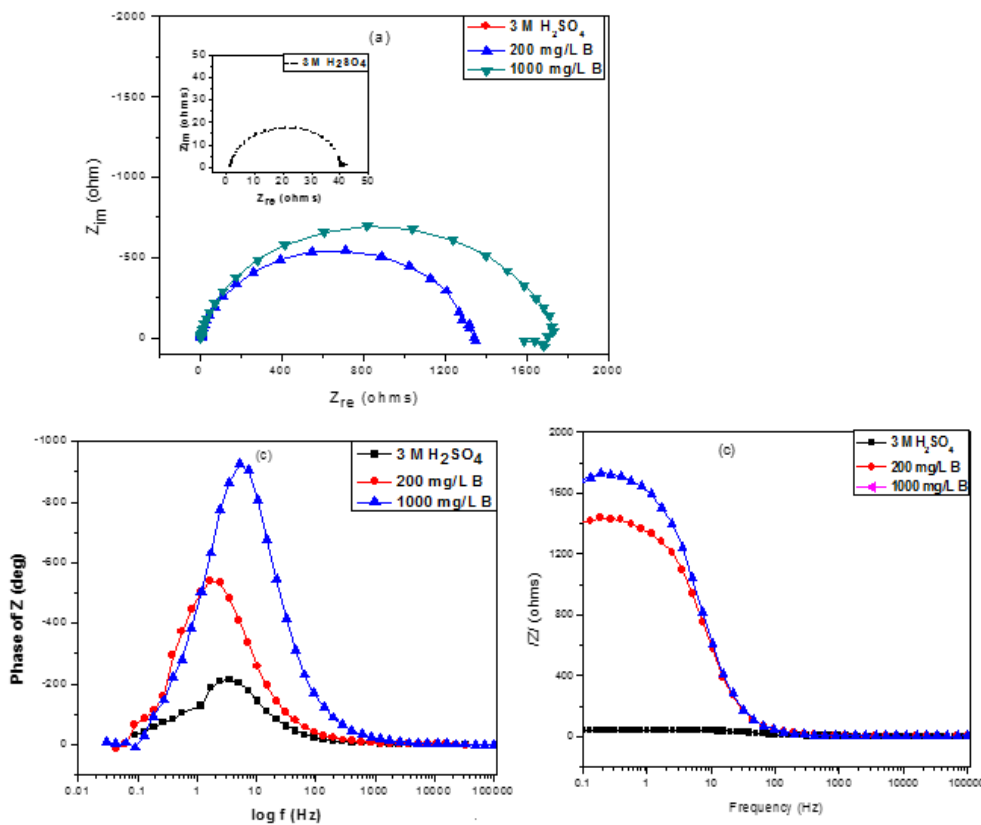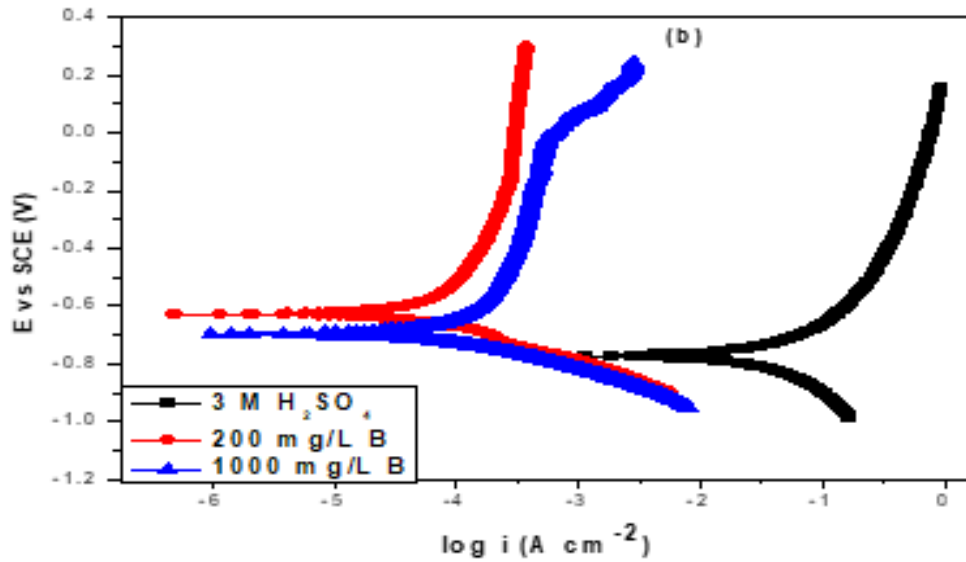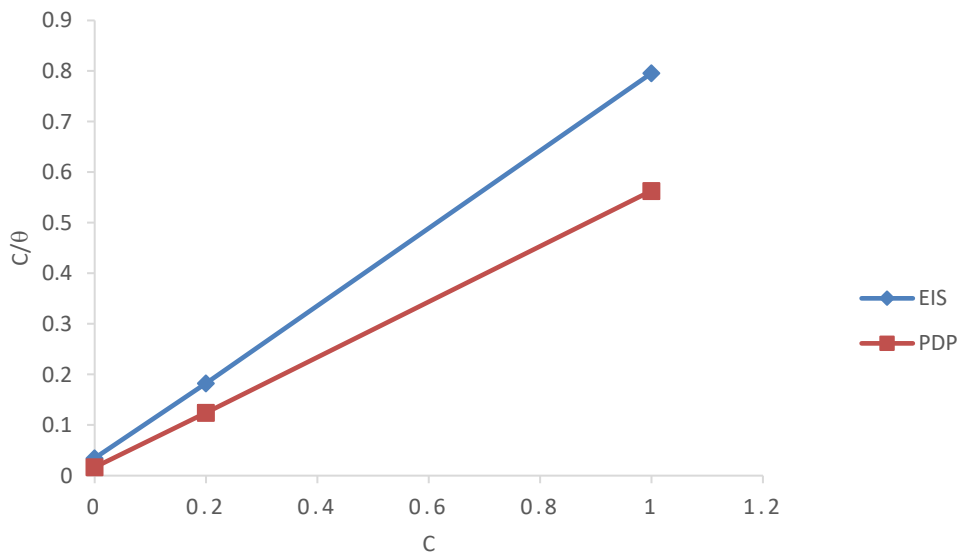

Fig. 3. (a) Nyquist plot, (b-c) Bode Impedance modulus and phase angle plots for mild steel in H$_2$SO$_4$ solution in the absence and presence of *B. eurycoma* leaves extracts

Table 2. Potentiodynamic polarization parameters for mild steel corrosion in H_2SO_4 solutions with and without different concentrations of *B. eurycoma* leaves extracts

System	$-E_{corr}$ vs SCE (mV)	I_{corr} ($\mu A/cm^2$)	β_a (V/dec)	β_c (V/dec)	$\eta_{Polarization}$ (%)
Blank	705.6 ± 37.1	265.2 ± 3.1	0.8 ± 0.03	0.2 ± 0.02	
200mg./L	752.3 ± 35.1	67.8 ± 0.2	0.25 ± 0.02	0.1 ± 0.01	80
1000mg/L	758.4 ± 33.6	48.0 ± 0.1	0.3 ± 0.01	0.1 ± 0.01	88

Fig. 4. Potentiodynamic polarization curves for mild steel in H_2SO_4 in the presence and absence of different concentration of B.*eurycoma* leaves extracts
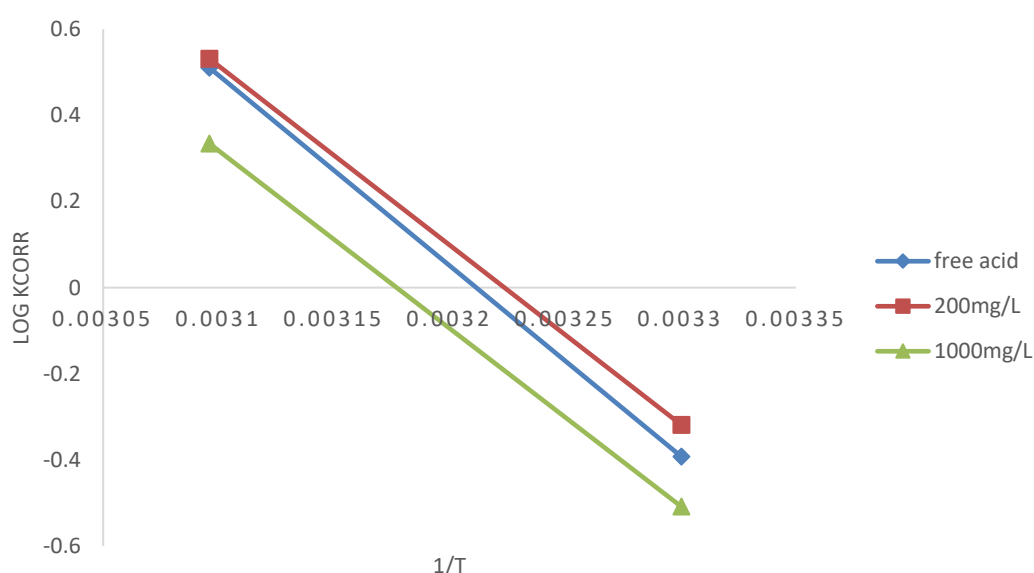

Fig. 5. Plot of Langmuir adsorption isotherm fitted on impedance value of mild steel in H_2SO_4 containing different concentrations of *B. eurycoma* leaves extract

Table 3. Langmuir's adsorption parameters for *B. eurycoma* leaves extract from 1 M H$_2$SO$_4$ on mild steel

Inhibitor Technique	Langmuir Adsorption Parameters			
	Slope	K$_{ads}$ (Lg^{-1})	-Δ_{Gads} (KJ mol^{-1})	R^2
EIS	0.0325	50.43	25.16	1.0000
PDP	0.0157	31.02	21.41	1.0000

Table 4. Thermodynamic adsorption parameters of B. eurycoma leaves extract adsorbed on the surface of MS in H2SO4 acid

Inhibitor	E$_a$ (KJ/mol)	A (g/cm^2/min)	ΔH* (KJ/mol)	ΔS* (J/mol/K)
Free acid	56.35	101.47	75.02	-168.86
B. eurycoma extract	29.32	102.64	22.09	-171.08

Fig. 6. Arrhenius plots for, MS in H$_2$SO$_4$ in the absence and presence of different concentrations of B. *eurycoma* leaves extract

$$logK_{corr} = log\left(\frac{R}{Nh}\right) + \frac{\Delta S^*}{2.303R} + \frac{\Delta H^*}{2.303RT} \quad (16)$$

Where h is Plank's constant, and N is Avogadro's number. Plotting of $logK_{corr}/T$ versus 1/T for the inhibitor gave a linear plot with intercept of $\left[ln\left(R/_{Nh} + \Delta S^*/_R\right)\right]$, from here ΔS^* were obtained, and the slope of $\left(-\Delta H^*/_R\right)$ gave the values of ΔH^* and listed in Table 4, Fig. 7.

The positive values of ΔH^* is an indication that the dissolution of MS is endothermic process and suggesting that the inhibitor was chemically adsorbed on the MS surface. The negative values of ΔS^* affirms that the rate determining step of the activated complex, is association and not dissociation.

Furthermore, the effect of temperature on the metal/acid solution interface plays an important role in evaluating the electrochemical corrosion reactions as a result of multifaceted alterations that occur on the metal surfaces due to relocation of the inhibitor molecules or break down, inhibitor molecule desorption and rapid etching [24]. Subsequently, changes in temperature affects dissolution of metals, inhibitor efficiency and inhibitor desorption/adsorption.

3.4 Surface Characterizations

3.4.1 FTIR analysis

Close examination of Fig. 8a reveals that the functional groups (O–H, C=O, C=N or C–O), of

B. eurycoma leaves extracts contain oxygen and nitrogen which is the backbone of corrosion *B. eurycoma* leaves extracts. The corrosion products on the mild steel surface immersed in 1 M H_2SO_4 containing inhibitor as seen on FTIR spectrum of Fig 8b has the absorption peaks of O–H, C=O/C=N, C–N, C–O–C which appeared at 3432 cm^{-1}, 1632 cm^{-1}, 1390 cm^{-1}, 1126 cm^{-1} correspondingly.

These observations can be accredited to the adherence of *B. eurycoma* leaves extracts on the mild steel surface. Again, looking at Fig 6a the band width of 3428 cm^{-1} with a broader curvature is attributable to the existence of molecular interactions was ascribed to the O–H stretching vibrations. Noticeable stretching vibration of C–H seen at 2931 cm^{-1} was accredited to C=O/C=N bending. The occurrence of absorption peaks at 1388 cm^{-1} and 1058 cm^{-1} can be attributed to stretching vibrations of C–N in the amides and C–O groups respectively [21].
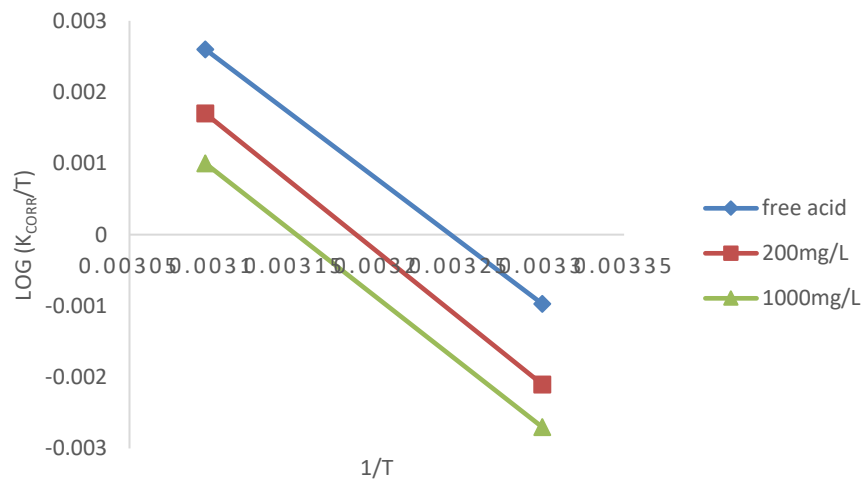

Fig. 7. Transition state plots (log k$_{corr}$/T vs. 1/T) for MS in H_2SO_4 in the absence and presence of different concentrations of B. *eurycoma* leaves extract
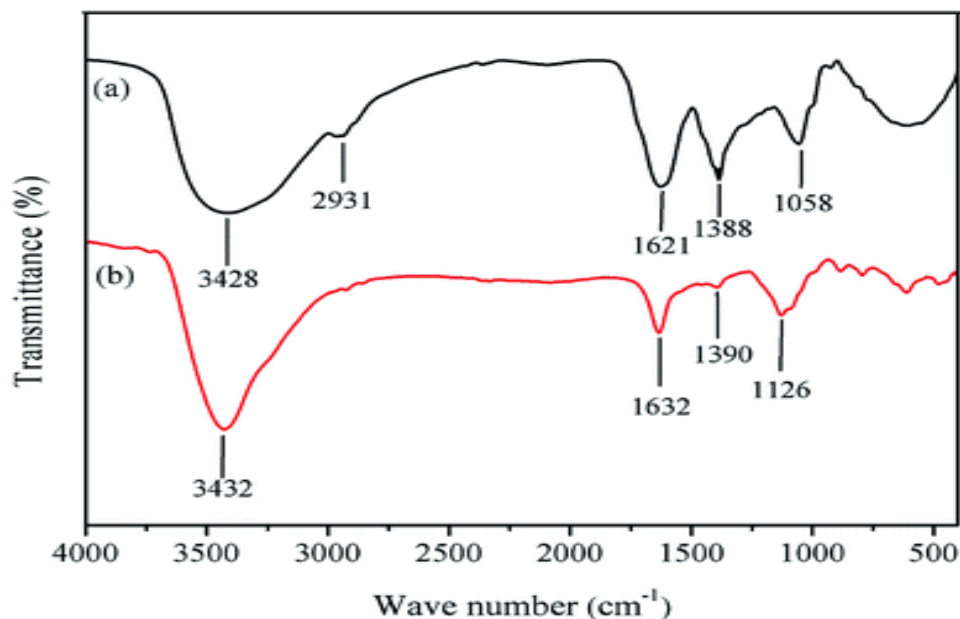

Fig. 8. FTIR spectra of (a) natural *B. eurycoma* leaves extracts and (b) *B. eurycoma* leaves extracts film adsorbed on the mild steel surface

3.4.2 SEM Inspection

Further insight was gained on the inhibitory properties of *B. eurycoma* leaves extracts by analyzing the surface morphology of mild steel with scan electron microscopy SEM. The SEM micrographs of mild steel surface after 8hrs in H_2SO_4 in the absence and presence of *B. eurycoma* leaves extracts were shown in Fig. 9. Critical inspection of Fig. 9b revealed profound gorges and big pits on the surface of mild steel in the absence of *B. eurycoma* leaves extracts, which differs greatly from the polished surface Fig. 9a. This can be attributed to the grave damage on the mild steel in 1 M H_2SO_4 solution. Although, it was clearly seen in Fig. 9c that the mild steel surface wears comparatively smoother morphology with 1000 mg L^{-1} *B. eurycoma* leaves extracts, which was identical to the polished surface. Additionally, the above occurrence suggests that the inhibitor molecules were adsorbed on the surface of mild steel to form a protecting film, which hindered the resultant corrosion from the aggressive solution to reach the metal surface. Therefore, the inhibitor glowingly shielded the mild steel from H_2SO_4 attack.

3.5 Quantum Calculations and Simulations Mechanism Considerations

Experimental findings were further investigated theoretically to ensure the existence of the adsorption of green inhibitors and their anticorrosion properties on the mild steel substrate under a different condition, by adopting MD simulations as active and reliable approach. Table 5 shows the energetic features of *B. eurycoma* leaves extracts. The obtained results in Table 5 revealed that the adsorption energies of the inhibitor molecules were negative, thereby attesting to the ability of selected molecules for adsorption over the iron. Fig 10 presents the side view of the snapshot from molecular dynamics model. It is observed from the configuration (Fig 10) that each dissolved molecule of the green inhibitor adhered to the surface of Fe (110). This theoretical result implies that there is the propensity of the inhibitor to form protective film on the mild steel substrates. Again, as can be seen from the top and side view snapshots that the molecular backbone of the surface-bound inhibitor depicts a flat– lying adsorption orientation with regard to the iron surface. This orientation increases contact with inhibitor and as a result significant increase in the degree of surface coverage and corrosion resistant properties of the inhibitor constituents studied. However, the properties calculated by quantum chemical approach, give information about reactivity of these molecules Table 4 but the reactivity cannot directly be translated to corrosion inhibition efficiency, which involves more processes such as competitive adsorption, etc. The adsorption energy (E_{ads}) which is important in characterizing the adsorption of these molecules onto the Fe surface was estimated using the Eq. (16) [10]
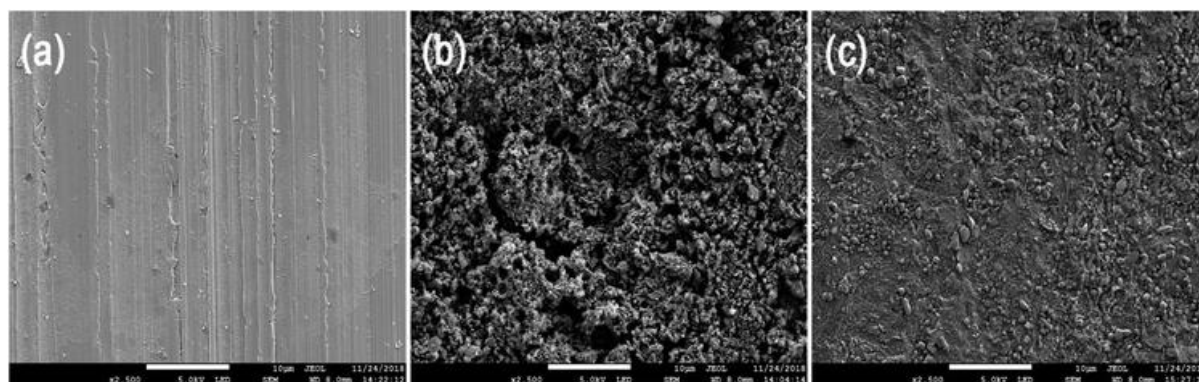

Fig. 9. SEM micrographs of mild steel (a) polished, (b) after immersion without and (c) with *B. eurycoma* leaves extracts

$$E_{ads} = E_{total} - \left(E_{surface+solution} + E_{inhibitor}\right) \ (16)$$

where $E_{inhibitor}$, $E_{surface + solution}$ and E_{total} represents the potential energy of a single molecule of these selected active components, the Fe slab without adsorption, and the total energy of the system containing a molecule and Fe surface, respectively. The negative values of adsorption energies indicate the adherence of inhibitive compounds onto the metallic (110) substrate.

It is well known from the electronic point of view that the adherence of corrosion inhibitors onto metallic surfaces is based on the donor – acceptor interaction [43-47]. Under such adsorption mechanism, the electron-rich centers of the inhibitors such as aromatic rings and oxygen heteroatoms donate their electrons to the vacant d orbitals of Fe atoms. Simultaneously, the inhibitor atoms can accept electrons from the filled orbitals of Fe atoms. Also, according to the frontier molecular orbital theory, it is evident that transfer of electronic charge which occur at inhibitor/metal interface is reliant on the highest occupied molecular orbital (HOMO) and lowest unoccupied molecular orbital (LUMO). The utmost ability of inhibitor to donate electrons through its energetic spot is depicted by HOMO whereas the LUMO presents the areas that accept electrons from HOMO of the metal cations Fig 10. Further calculations on the electron/atoms of the inhibitor molecules were done with the density functional theory DFT/B3LYP method [48 -51] to clarify more on HOMO and LUMO as well as the geometrics of *B. eurycoma* inhibitor. It is possible from Fig. 10 that the HOMO can be traced closely to the benzene ring and its adjoining methoxy group and carbonyl oxygen and C=C double bonds, whereas on the other hand the LUMO occurs on the carbon atoms of aromatic rings and the energetic carbonyl spots. Since there is the presence of methoxy in conjunction with carbonyl oxygen centers, aromatic benzene rings as well as the double bonds of C=C, these can donate their electrons to the void d orbitals of the surface

Fe atoms, and as result interact with the surface metal cation by mechanism of donor-acceptor process. This can be attributed to the fact that the HOMO electrons are seen above the aromatic circles or rings and on the carbonyl O atoms suggesting that the inhibitor can part with some of its delocalized π electron of aromatic circles and electron pairs of oxygenated energetic spots to vacant orbitals in the surface of metal cations. Again, investigation of the inhibitor geometry indicate that the HOMO orbital was dispensed above the circles and nearly on hydroxyl oxygen but the LUMO appeared on the middle circles. As evidenced in the Homo of DFT/B3LYP, the species can be found on the carbonyl bond and its surrounding cycle comprising of C=C double bonds, which implies donation of elections from the sensitive lively spots. Additionally, the pictorial view of HOMO and LUMO of *B. eurycoma* substance, it is obvious that the electron-rich benzene ring, C=C double bond as well as oxygen heteroatoms performed as the sensitive areas for HOMO thereby presenting their strong propensity for transferring of electrons to the surface of metal cation. Also, Fig. 10 shows the electronic properties of N-methyl-3,4 methylenedioxy phenylpropan-3-amine which is a major component of *B. eurycoma* substance.

The global reactivity indices were elucidated via some inherent quantum chemical parameters which include energetics of molecular orbitals (i.e. E_{L-H} gap, E_{LUMO} and E_{HOMO}), electronic affinity, ionization potential, electronegativity, hardness and fracture of electronic charge transferred between the metal surface and the natural inhibitor etc. were considered and the quantitative values are presented in Table 6. It is obvious from Table 6 that the low negative HOMO energy provides more charges to the vacant d orbitals of Fe cations. This can be attributed to the reduced energy gap (E_{L-H}) which provides development to strengthen charge sharing at the interface of inhibitor/metal resulting to intensified interactions [52-53].

Table 5. The energetic descriptors and outputs of *B. eurycoma* leaves extracts over Fe 110
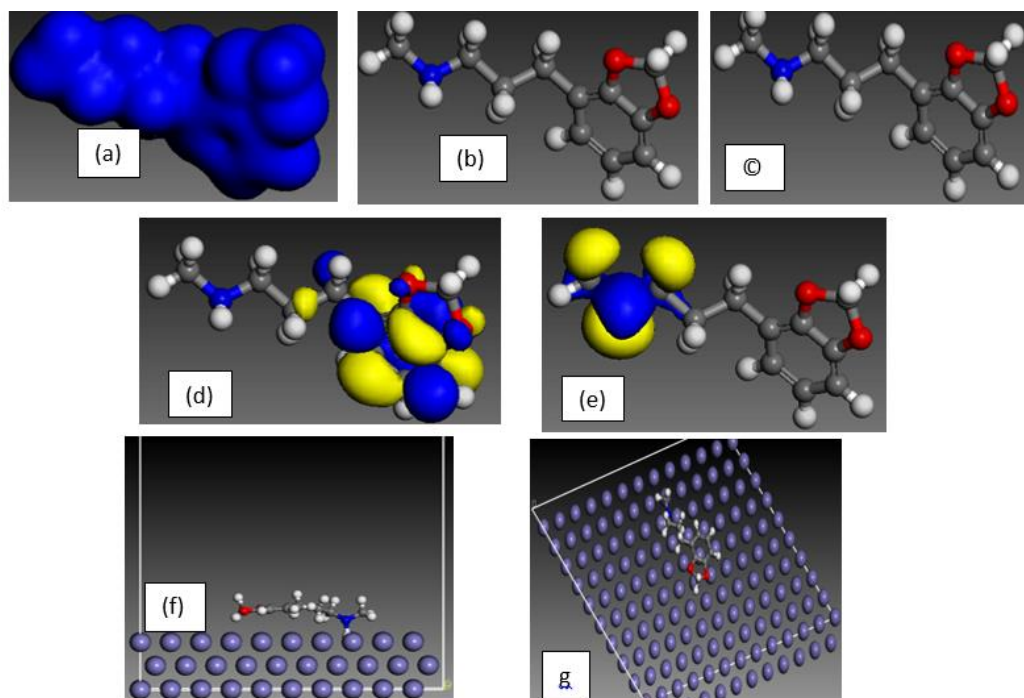
Descriptors (kcal/mol)	Outputs
Total energy	-330.447
Adsorption energy	-199.332
Rigid adsorption energy	-197.848
Deformation energy	-1.822
dE_{ads}/dN_i	-199.332

Table 6. Calculated quantum chemical parameters

Inhibitor	E_H	E_L	ΔE_{L-H}	A	I	χ	η	ΔN
B. eurycoma	-6.860	-2.810	4.080	2.810	6.860	4.835	1.858	0.540

Furthermore, Fukui indices for electrophilic and nucleophilic performance for the studied inhibitor was analyzed by considering the sensitive (reactive) energetic spot of the *B. eurycoma* inhibitor in acidic medium and presented in Fig. 8. It is observable from the Fig. 8 that the C=C double bond, aromatic circles, and carbonyl oxygen as well as methoxy presented electrophilic behavior corresponding to HOMO results thereby confirming the propensity to donate electron to the surface of Fe atoms with unfilled d orbitals [54]. Then, the carbonyl group, the carbon atoms above the circles and those in the double bond depicts nucleophilic behavior. Like the molecular orbital distribution the carbonyl O atoms, benzene ring as well as the heterocyclic atoms performed as energetic spot for adsorption through electrophilic style thereby replicating their ability to provide electrons to the surface Fe cations, on the other hand, the ring

carbon atoms acts as nucleophilic areas. Geometrically, it is possible that the minimum energy of acid inhibitor behaving in a nucleophilic manner can occur on hydroxyl O atom, while another hydroxyl oxygen and carbon atoms in close proximity acts like an energetic spot for nucleophilic attack of the inhibitor leading to donor- acceptor interactions due to the acceptance of electrons from filled orbital surface metal atoms [53-55]. Inspection of Fukui indices for electrophilic behavior of *B. eurycoma* inhibitor indicate that corrosion inhibition occurred between the heterocyclic O atom and aromatic rings or circles. This validates the HOMO results which is an indicative of the inhibitor binding to the surface of Fe (110) due delocalization of π electrons from lone pair electrons and aromatic rings to vacant d orbitals.
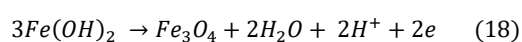

Fig. 10. Electronic properties of N-methyl-3,4 methylenedioxy phenylpropan-3-amine (a) Electron density, (b) electrophilic f (-), (c) nucleophilic f (+), (d) HOMO, (e) LUMO (f) side view of the snapshot for N-methyl-3,4 methylenedioxy phenylpropan-3-amine from molecular dynamics model. (g) top view of the Snapshot for N-methyl-3,4 methylenedioxy phenylpropan-3-amine from molecular dynamics model. Atom legend: white = H; gray = C; red = O. The blue and yellow isosurfaces depict the electron density difference: the blue regions show electron accumulation while the yellow regions show electron loss

Table 7. Inhibition efficiency of B. eurycoma compared to that of other inhibitors reported

Inhibitor	Metal/Medium	Inhibition efficiency	Inhibitor's concentration	Corrosion density reduction	References
B. eurycoma leaves extract	Mild steel/acidic	88%	1000 mg/l	From 265.2 μA/cm^2 to 67.8 μA/cm^2 (74.43%)	This work
Dialium guineense leaf extract	Mild steel/alkaline	78%	1 g/l	-	[24]
Kalmegh leaf extract	Aluminum/alkaline	82.45%	1 g/l	96.3 mA/cm^2 to 16.9 mA/cm^2 (82.45%)	[2]
Nonanedihydrazide	Mild steel/acidic	97%	-	667 μA/cm^2 to 44.62 μA/cm^2 (93.31%)	[38]
Cnidoscolus aconitifolius leaves extract	Mild steel/acidic	96.9%	4 g/l	2571.1 μA/cm^2 to 219.9 μA/cm^2 (91.45%)	[26]

3.6 Corrosion Mechanism

In the current work, the major effect in the corrosion inhibition of mild steel by *B. eurycoma* leaves extracts is attributed to hydrogen ion concentration (pH). It is quite understandable that the Potential-pH equilibrium of metals varies according to aqueous media it is subjected to. As a result, mild steel experiences uniform corrosion at low pH environment (acid). On the other hand, a ferrous hydroxide $Fe(OH)_2$ is formed at high pH (6-7), the formed $Fe(OH)_2$ is enclosed by a steady layer of magnetite Fe_3O_4 produced on the iron surface which retard the influence of corrosion on the surfaces covered but can result to localized corrosion surfaces not affected.

$$Fe^{2+} + 2H_2O \rightarrow Fe(OH)_2 + 2H^+ \qquad (17)$$

$$3Fe(OH)_2 \rightarrow Fe_3O_4 + 2H_2O + 2H^+ + 2e \qquad (18)$$

$$2H^+ + 2e^- \rightarrow H_2 \qquad (19)$$

$$3Fe(OH)_2 \rightarrow Fe_3O_4 + 2H_2O + H_2 \qquad (20)$$

The data obtained from this work reveals that the inhibition efficiency of mild steel by *B. eurycoma* leaves extract rises as the pH level reduces. This can be attributed to the formation of a protective film created by the adsorption of *B. eurycoma* leaf extract on steel surface which prohibited the effect of H$^+$ ion and the dissolution of mild steel [3].

3.7 Comparison of Inhibitive Capability of *B. eurycoma* Leaves Extract with that of Other Inhibitors

Table 7 shows a comparison of inhibition efficiency for *B. eurycoma* leaves extract with that of other inhibitors. The comparison is non-exhaustive and only an indication of the range of inhibition efficiency as the experimental conditions (inhibitor's concentration, contact time, temperature etc.) and environment (acidic or alkaline) among the studies are different. Nevertheless, inhibitive capability of *B. eurycoma* leaves extract for mild steel in acidic medium is comparatively good.

4. CONCLUSION

This work evaluated the inhibitory action of *B. eurycoma* leaves extracts for mild steel in H$_2$SO$_4$ solution and conclude thus:

- The inhibition efficiency for mild steel corrosion in 1 M H$_2$SO$_4$ increased with increase in the inhibitor concentration. The inhibition ability of the leaf's extract with respect to EIS and PDP were 85% and 88% respectively. This was validated through surface analyses from SEM.
- The inhibitor performed as mixed-type inhibitor by merely hindering the anodic

and cathodic energetic sites without changing the corrosion mechanism.

- The obtained C_t data reduced appreciably with increase in the concentration of the inhibitor due to adherence of thick oxide layer on the MS surface
- The adsorption of the extracts obeyed the Langmuir adsorption isotherm, and the free energy of adsorption indicated a mixed type of adsorption for the inhibitor species on the metal surface.
- The SEM and FT-IR techniques confirmed the formation of the adsorbed film. The adsorbed layers exhibited effective anti-corrosion behavior
- Also, the adsorption of the extracts unto MS surface leads to significant rise in the parallel mode as well as in the number of reactive sites in the molecular structures.

COMPETING INTERESTS

Authors have declared that no competing interests exist.

REFERENCES

1. Dehghani, et al, A combined experimental and theoretical study of green corrosion inhibition of mild steel in HCl solution by aqueous Citrullus lanatus fruit (CLF) extract, Journal of Molecular Liquids; 2019.
Available:https://doi.org/10.1016/j.molliq.2019.02.010
2. Namrata, et al. Electrochemical approach of Kalmegh leaf extract on the corrosion behavior of aluminum alloy in alkaline solution, International journal of Industrial Chemistry. 2017;8:75-82.
Available:https://doi.org/10.1007/s40090-016-0103-y
3. Onyenanu, et al, Corrosion Inhibition potentials of *A. mossambicensis* and *E. sonchifolia* Leaves' Extracts on Aluminum in Alkaline Media: Insights from Gravimetric and Electrochemical Studies, Chemistry Africa; 2022.
Available:https://doi.org /10.1007/s42250-022-00531-0
4. Eiman, et al, Glycyrrhiza glabra leaves extract as a green corrosion inhibitor for mild steel in 1 M hydrochloric acid solution: Experimental, molecular dynamics, Monte Carlo and quantum mechanics study. J Mol Liq. 2018;255:185–198.
Available:https://doi.org/10.1016/j.molliq.2018.01.144
5. Turuvekere, et al. Evaluation of newly synthesized hydrazones as mild steel corrosion inhibitors by adsorption, electrochemical, quantum chemical and morphological studies, Arab Journal of Basic and Applied Sciences. 2018;25(2):45-55.
DOI: 10.1080/25765299.2018.1449347
6. Olofinjana, et al. Quantum chemical studies on corrosion inhibition of 1, 3-thiazine derivatives for mild steel in acidic media: DFT approach. Manila Journal of Science. 2017;10:44-63.
7. Sam John, et al. Corrosion inhibition properties of 1, 2, 4-Hetrocyclic Systems: Electrochemical, theoretical and Monte Carlo simulation studies, Eyptian Journal of Petroleum. 2017;26(3):721-732.
Available:https://doi.org/10.1016/j.ejpe.2016.10.005
8. Tsoeunyane, et al. Corrosion Inhibition of Mild Steel by Poly(butylene succinate)-L-histidine Extended with 1,6-diisocynatohexane Polymer Composite in 1 M HCl. International Journal of Corrosion; 2019.
Article ID 7406409
Available:https://doi.org/10.1155/2019/7406409
9. El-Shamy, et al. Optimization of the influencing variables on the corrosion property of steel alloy 4130 in 3.5 wt.% NaCl Solution. Journal of Chemistry; 2020.
Article ID 9212491.
Available:https://doi.org/10.1155/2020/9212491
10. Barbouchi, et al. Theoretical and experimental studies of lentisk leaf extract as green corrosion inhibitor for Iron in chloride media. Biointerface Research in Applied Chemistry. 2023;13(6).
Available:https://doi.org/10.33263/BRIAC136.557
11. Hsissou, et al. Insight into the corrosion inhibition of novel macromolecular epoxy resin as highly efficient inhibitor for carbon steel in acidic mediums: Synthesis, characterization, electrochemical techniques, AFM/UV–Visible and computational investigations. J. Mol. Liq. 2021;337.
Available:https://doi.org/10.1016/j.molliq.2021.116492
12. Verma, et al. 5-(Phenylthio)-3H-pyrrole-4-carbonitriles as effective corrosion inhibitors for mild steel in 1 M HCl: Experimental and theoretical investigation.

Journal of Molecular Liquids. 2015;212:209–218.
Available:https://doi.org/10.1016/j.molliq.2015.09.009

13. Verma, et al. A thermodynamical, electrochemical and surface investigation of Bis (indolyl) methanes as Green corrosion inhibitors for mild steel in 1 M hydrochloric acid solution, Journal of the Association of Arab Universities for Basic and Applied Sciences. 2016;21:24 –30.
DOI: 10.1016/j.jaubas.2015.04.003

14. Manh, et al. Corrosion Inhibition of Mild Steel in Hydrochloric Acid Environments Containing Sonneratia caseolaris Leaf Extract, ACS Omega. 2022;8874-8886.
Available:https://doi.org/10.1021/acsomega.1c07237

15. Fouda, et al. Novel pyrimidine-bichalcophene derivatives as corrosion inhibition for copper in 1M nitric acid solution, RSC Advances. 2021;11(41):25314-25333.
DOI: 10:1039/d1ra03603c

16. Al-Moubaraki, Al-Malwi. Experimental and theoretical evaluation of aqueous black mustard seeds extract as sustainable-green inhibitor for mild steel corrosion in H_2SO_4 acid solutions. Journal of Adhesion Science and Technology. 2022;36(23-24)2612-2643.
DOI: 10.1080/01694243.2022.2062955

17. Dongyi, et al. The inhibition of mild steel corrosion in 1 M H_2SO_4 solution by radish leaf extract, Royal Society of Chemistry Advances. 2019;9:40997-41009.
DOI: 10.1039/C9RA04218K

18. Bahlakah, et al. Experimental and theoretical studies of the synergistic inhibition effects between the plant leaves extract (PLE) and zinc salt (ZS) in corrosion control of carbon steel in chloride solution, Journal of molecular liquids. 2017;248:845-870.
Available:https://doi.org/10.1016/j.molliq.2017.10.120

19. Emembolu, et al. Electrochemical and statistical study of the inhibition effect of T. conophorum leaf extract on aluminum corrosion in acidic medium, Safety in Extreme Environments; 2021.
Available:https://doi.org/10.1007/s42797-021-00040-2

20. Hammud, et al. An integrated experimental and theoretical studies on the corrosion inhibition of carbon steel by harmal extracts, Molecules. 2022;27(21):7250.

Available:https://doi.org/10.3390/molecules27217250

21. Ojha, et al. Experimental and theoretical study of effect of *allium sativum* extracts as corrosion inhibitor on mild steel in 1 m HCL medium. J Bio Tribo Corros. 2020;39(6).
Available:https://doi.org/10.1007/s40735-020-00336-z

22. Haldhar, et al. Experimental and theoretical studies of ficus religiosa as green corrosion inhibitor for mild steel in 0.5 m h2so4 solution. Sustainable Chemistry and Pharmacy. 2018;9:95-105.
Available:https://doi.org/10.1016/j.scp.2018.07.002

23. Loto RT. Electrochemical analysis of the corrosion inhibition properties of 4-hydroxy-3-methoxybenzaldehyde on low carbon steel in dilute acid media. Cogent Engineering. 2016;3(1):242 -107.
Available:http://dx.doi.org/10.1080/23311916.2016.1242107

24. Emembolu LN, Achugbu Obioma OD, Onukwuli. Bioinhibition of corrosion of mild steel in 1 m naoh by ethanolic extract of *Dialium guineense* Leaves Using Different Corrosion Techniques, Manila Journal of Science. 2022;15(2):1-18.

25. Qusay Jawad A, Dhafer Zinad S, Rawaa Dawood Salim, Ahmed A Al-Amiery, Tayser Sumer Gaaz, Mohd S, Takri, Abdul H, Amir Kadhum, Synthesis, Characterization, and Corrosion Inhibition Potential of Novel Thiosemicarbazone on Mild Steel in Sulfuric Acid Environment, Coatings. 2019;9.
DOI: 10.3390/coatings9110729

26. Ugi BU, Uwah IE, Okafor PC. Sulphuric acid corrosion of mild steel in leave extracts of cnidoscolus aconitifolius plant. Chemical and Process Engineering Research. 2016;46:35-41.

27. Pandian BR, Afidah AR, Hasnah O, Khalijah A. Inhibitive effect of Xylopia ferruginea extract on the corrosion of mild steel in 1M HCl medium, International Journal of minerals, metallurgy, and materials. 2011;18:413-418.
Available:https://doi.org/ 10.1007/s12613-011-0455-4

28. Emembolu, et al. Evaluation of the corrosion inhibitory effect of *Napoleonaea imperalis* leaf extract on mild steel in 1.3 M H2SO4 medium, Journal of Bio- and Tribo-corrosion. 2020;6(128):1-15.
Available:https://doi.org/10.1007/s40735-020-00422-2

29. Shehata, et al. Crispy dry chili extract as an eco-friendly corrosion inhibitor for mild steel in chloride solutions: Experimental and theoretical studies. Journal of Bio- and Tribo-Corrosion. 2022;8(97).
Available:https://doi.org/10.1007/s40735-022-00691-z

30. Emori, et al. Adsorption and corrosion inhibition performance of multi-phytoconstituents from dioscorea septemloba on carbon steel in acidic media: Characterization, experimental and theoretical studies. Colloids and Surfaces A: Physicochemical and Engineering Aspects. 2020;590:124-534.
Available:https://doi.org/10.1016/j.colsurfa.2020.124534

31. Liu, et al. Corrosion protection for mild steel by extract from the waste of lychee fruit in HCl solution: Experimental and theoretical studies. Journal of Colloid and Interface Science. 2018;520:41-49.
Available:https://doi.org/10.1016/j.jcis.2018.02.071

32. Haldhar, et al. *Valeriana wallichii* root extract as a green and sustainable corrosion inhibitor for mild steel in acidic environments: Experimental and theoretical study, Materials Chemistry Frontiers. 2018;2:1225-1237.
DOI: 10.1039/C8QM00120K

33. Vorobyova, Skiba. Peach pomace extract as novel cost-effective and high-performance green inhibitor for mild steel corrosion in NACL solution: Experimental and theoretical research. Waste and Biomass Valorization. 2021;12:4623–4641.
Available:https://doi.org/10.1007/s12649-020-01333-6

34. Yaxu, et al. Orange peel extracts as biodegradable corrosion inhibitor for magnesium alloy in NaCl solution: Experimental and theoretical studies. Journal of the Taiwan Institute of Chemical Engineers. 2020;115:35-46.
Available:https://doi.org/10.1016/j.jtice.2020.10.010

35. Daniel, et al. Exploring the efficacy of phytoconstituents from *Vernonia amygdalina* on mild steel protection in acid environment: Combined experimental and theoretical study. Journal of Bio- and Tribo-Corrosion. 2021;7(126).
Available:https://doi.org/10.1007/s40735-021-00562-z

36. Haldhar, et al. Experimental and theoretical evaluation of *Acacia catechu* extract as a natural, economical and effective corrosion inhibitor for mild steel in an acidic environment. Journal of Bio- and Tribo-Corrosion. 2020;6(76).
Available:https://doi.org/10.1007/s40735-020-00368-5

37. Liu, et al. Longan seed and peel as environmentally friendly corrosion inhibitor for mild steel in acid solution: Experimental and theoretical studies. Journal of Colloid and Interface Science. 2017;499:110-119.
Available:https://doi.org/10.1016/j.jcis.2017.03.091

38. Al-Amiery, et al. Experimental and theoretical study on the corrosion inhibition of mild steel by nonanedioic acid derivative in hydrochloric acid solution. Journal of Scientific Reports. 2022;12: 4705.
Available:https://doi.org/10.1038/s41598-022-08146-8

39. Olasehinde, et al. Corrosion inhibition of mild steel in 1 m HCL by methanolic *Chromolaena odorata* leaf extract: Experimental and theoretical studies. Journal of Bio- and Tribo-Corrosion. 2022;8:105.
Available:https://doi.org/10.1007/s40735-022-00704-x

40. Anupama, Joseph. Xperimental and theoretical studies on *Cinnamomum verum* leaf extract and one of its major components, eugenol as environmentally benign corrosion inhibitors for mild steel in acid media. Journal of Bio- and Tribo-Corrosion. 2018;4:30.
Available:https://doi.org/10.1007/s40735-018-0146-z

41. Emembolu, Igbokwe. Inhibition capability of *Dennettia tripetala* leaves extract on low carbon steel in 4 m HCL solutions. Journal of Basic and Applied Research International. 2020;26(1):23-35.

42. Deyab, et al. Aesculus hippocastanum seeds extract as eco-friendly corrosion inhibitor for desalination plants: Experimental and theoretical studies. Journal of Molecular Liquids. 2022;361: 119594.
Available:https://doi.org/10.1016/j.molliq.2022.119594

43. Cheng, et al. Corrosion inhibition of copper in sulfuric acid by Leonurus japonicus houtt. Extract as a green corrosion inhibitor: Combination of experimental and theoretical research. Journal of the Taiwan Institute of

Chemical Engineers. 2022;139:104532.
Available:https://doi.org/10.1016/j.jtice.20
22.104532

44. Rani, et al. Inhibition of mild steel corrosion in HCl using aqueous and alcoholic extracts of Crotalaria Pallida – A combination of experimental, simulation and theoretical studies. Journal of Molecular Liquids. 2021;334:116515.
Available:https://doi.org/10.1016/j.molliq.2
021.116515

45. Zerroug, et al. Experimental and theoretical evaluation of the adsorption process of some polyphenols and their corrosion inhibitory properties on mild steel in acidic media. Journal of Environmental Chemical Engineering. 2021;9(6):106482.
Available:https://doi.org/10.1016/j.jece.20
21.106482

46. Rajesh, et al. Armoracia rusticana as sustainable and eco-friendly corrosion inhibitor for mild steel in 0.5M sulphuric acid: Experimental and theoretical investigations. Journal of Environmental Chemical Engineering. 2018;6(4):5230-5238.
Available:https://doi.org/10.1016/j.jece.20
18.08.025

47. Nor et al. Environmentally conscience corrosion inhibitors for mild steel in corrosive hydrochloric acid solution by *Uncaria Cordata* extract: Experimental and theoretical studies. Journal of Adhesion Science and Technology; 2020.
Available:https://doi.org/10.1080/01694243
.2023.2196905

48. Anis, et al. Experimental and theoretical study of polysaccharides extracted from prickly pear nopales Pulp (PPUN) of Opuntia ficus-indica as corrosion inhibitors. Journal of Molecular Liquids. 2023;384:122272.
Available:https://doi.org/10.1016/j.molliq.20
23.122272

49. Sadegh, et al. Comprehensive assessment of some l-amino acids as eco-friendly corrosion inhibitors for mild steel in HCl: Insights from experimental and theoretical studies. Journal of Physics and Chemistry of Solids. 2023;181:111550.
Available:https://doi.org/10.1016/j.jpcs.202
3.111550

50. Fouda, et al. Nano-metal-organic frameworks as corrosion inhibitors for strengthening anti-corrosion behavior of carbon steel in a sulfuric acid environment: from synthesis to application, RSC Adv. 2023;15222.
DOI: 10:1039/d3ra01644g

51. Al-Moubaraki. Potential of borage flowers aqueous extract, *Borago officinalis L*., against the corrosion of mild steel in phosphoric acid. Journal of Anti-Corrosion Methods and Materials. 2018;65(1): 53-65.
Available:https://doi.org/10.1108/ACMM-
04-2017-1788

52. Al-Moubaraki, et al. Development of natural plant extracts as sustainable inhibitors for efficient protection of mild steel: Experimental and first-principles Multi level computational methods, Materials. 2022;15(23):8688.
Available:https://doi.org/10.3390/ma15238
688

53. Baskar P, Rathinapriya P, Prabakaran M. Use of trochodendron aralioides extract as green corrosion inhibitor for mild steel in 1m Hcl solutions. Processes. 2022;10: 1480.
Available:https://doi.org/10.3390/pr100814
80

54. Emembolu, et al. Comparison of RSM and ANFIS modeling techniques in corrosion inhibition studies of *Aspilia Africana* leaf extract on Mild steel and Aluminium metal in acidic medium. 2022;11.
Available:https://doi.org/10.1016/j.apsadv.2
022.100316

55. Soltani, Khayatkashani. Gundelia Tournefortii as a Green Corrosion Inhibitor for Mild Steel in HCl and H2SO4 Solutions. Int. J. Electrochem. Sci. 2015;10:46–62.
Available: https://doi.org/10.1016/S1452-
3981(23)04974-X

Peer-review history:
The peer review history for this paper can be accessed here:
https://www.sdiarticle5.com/review-history/116851